The effect of impedance on interaural azimuth cues derived from a spherical head model[a)]

Bradley E. Treeby,[b)] Roshun M. Paurobally, and Jie Pan
Centre for Acoustics, Dynamics and Vibration, School of Mechanical Engineering, The University of Western Australia, 35 Stirling Highway, Crawley, WA 6009, Australia

(Received 15 June 2006; revised 24 January 2007; accepted 26 January 2007)

Recent implementations of binaural synthesis have combined high-frequency pinna diffraction data with low-frequency acoustic models of the head and torso. This combination ensures that the salient cues required for directional localization in the horizontal plane are consistent with psychophysical expectations, regardless of the accuracy or match of the high-frequency cues, or the fidelity of experimental low-frequency information. This paper investigates the effect of a nonrigid boundary condition on the surface pressure and the resulting interaural cues used for horizontal localization. These are derived from an analytical single sphere diffraction model assuming a locally reacting and uniformly distributed impedance boundary condition. Decreasing the magnitude of a purely resistive surface impedance results in an overall decrease in the sphere surface pressure level, particularly in the posterior region. This produces nontrivial increases in both the interaural level and time difference, especially for sound source directions near the interaural axis. When the surface impedance contains a reactive component the interaural cues exhibit further changes. The basic impedance characteristics of human hair and their incorporation into the sphere diffraction model are also discussed. © *2007 Acoustical Society of America.* [DOI: 10.1121/1.2709868]

PACS number(s): 43.66.Pn, 43.66.Qp, 43.20.Fn [AK] Pages: 2217–2226

I. INTRODUCTION

Typical implementations of virtual audio systems combine acoustic signals with head related transfer functions (HRTFs) to artificially position sounds within a virtual three-dimensional (3D) environment. The HRTF itself is a measure of the combined diffraction properties of the exterior human acoustic system, and generally reflects the spectral changes that a plane sound wave from a particular source direction would undergo by the time it reaches the eardrums. Extensive localization testing in recent years has highlighted the importance of using HRTFs that are accurately matched to the individual users so that the auditory cues required for a realistic and spatially accurate acoustic environment are maintained. The use of nonindividualized HRTFs generally results in decreased spatial accuracy amongst other common error artifacts, although the extent depends on the degree of mismatch between the end user and the HRTF data utilized (Wenzel *et al.*, 1993; Bronkhorst, 1995). The availability of laboratory environments equipped to measure personalized HRTF sets is exceptionally limited; thus many recent implementations have instigated solutions which attempt to provide a better match between the end user and the nonindividualized HRTF set used. Amongst others these methods include selecting the HRTF set based on anthropometric similarities between the user and a database of previously measured users (Zotkin *et al.*, 2003), frequency scaling of the HRTF based on pinna characteristics (Middlebrooks, 1999), and allowing the user a choice of standard HRTFs based on personal preference of the quality of the virtual projection (Middlebrooks *et al.*, 2000). In particular, implementations combining an analytical low-frequency head, or head-and-torso, model with the high-frequency pinnae data of the HRTF have had particular success (Brown and Duda, 1998; Algazi *et al.*, 2002a; b). These composite HRTFs progressively replace cues with those derived from the analytical model for frequencies below 3000 Hz (below 500 Hz the model is used exclusively). The models can be modified to suit the anthropometry of the end user (Algazi *et al.*, 2001), and provide stable azimuth cues and trends consistent with psychophysical expectations regardless of the coherence of the low-frequency component of the HRTF, or the accuracy of the match between the spectral pattern provided by the users own pinnae and the high-frequency data used.

This paper provides a comprehensive investigation into the effect of altering the surface boundary condition of a low-frequency head model on the surface pressure and the salient azimuth cues [interaural time difference (ITD) and interaural level difference (ILD)]. These are derived from an analytical head model based on diffraction around a single sphere with a uniformly distributed and locally reacting impedance boundary. The analytical diffraction solution is presented and subsequently experimentally validated. The effect of varying the surface impedance on the corresponding surface pressure over the frequency range of interest for head-and-torso models (below 3000 Hz) is then investigated. These results are used to examine the general trends experienced by the interaural difference cues with impedance. Dis-

[a)]Portions of this work were presented in "Investigation of the effect of impedance on azimuth cues derived from spherical head models," Proceedings of the 12th International Conference on Auditory Display, London, UK, 20–23 June, 2006.

[b)]Electronic mail: treebs@mech.uwa.edu.au

cussion relating to the effect of human hair impedance on the interaural cues (based on the same boundary condition assumption) is also given.

Although mathematical solutions for a locally reacting and uniformly distributed impedance boundary condition have been previously published (Lax and Feshbach, 1948; Kear, 1959; Morse and Ingard, 1968), such treatments have generally not been utilized in virtual acoustics. In this regard derivations and discussions are overwhelmingly based on rigid boundary conditions and cannot be trivially expanded to include an acoustic impedance term (the assumption of an acoustically rigid boundary allows noticeable simplification of the analytical diffraction solution). Most commonly the models used are simply a single pinnae-less rigid sphere with its diameter matched to the inter-ear distance of the user, although more recent implementations have combined this with a separated spherical torso to include a low-frequency approximation of the secondary information introduced by upper torso reflections (Gumerov and Duraiswami, 2002; Algazi *et al.*, 2002a). The principal analytic results for the model utilized in the current study are thus also included in this paper.

Previous experimental studies have illustrated changes in the HRTF and interaural cues with varying the surface boundary conditions. Kuhn (1977) compared measurements from a mannequin (with a torso) with and without clothing and concluded that the interaural cues changed with this modification. For small angles of head rotation relative to the torso (which was held constant relative to the source angle) this study reported variability in the ILD and ITD over frequency (260–4000 Hz) of up to 5 dB and 50 μs, respectively. Riederer (2005) also investigated the effect of hair and hair style changes on the resultant HRTF using a mannequin fitted with a variety of wigs. The effect of the hair thickness and curliness appeared to be the most prominent (subsequent modification of hair style or changes in overall hair length reportedly had a much smaller effect) and produced an increased shadowing effect of the incident wave, with changes in the HRTF above 2 kHz on the order of 5 dB. Studies utilizing boundary element models incorporating nonrigid head surfaces have shown similar results; Katz (2001) reported up to 6 dB difference in the HRTF generated due to the inclusion of hair characteristics based on a locally reactive boundary condition, the effects again being most pronounced in the rear (shadowed) region of the head.

The lack of consideration for nonrigid acoustic boundary conditions in analytical auditory cue investigations may also be attributed to both the variability and the general absence of data on the acoustical properties of the various surfaces that constitute the human head and torso. This is in part due to the lack of experimental techniques available to take *in situ* measurements of impedance from human subjects. Limited previous studies have provided absorption coefficient data obtained using an impedance tube for both human skin (found to be approximately rigid in the frequency range of interest) and hair (Katz, 2000). In the case of hair, additional difficulty arises in accurately describing a boundary condition to embody the diverse range of hair densities, lengths, distributions, and fiber shapes. While the current work does not attempt to formulate a model to address this issue, it does give an indication of the level of changes expected from more detailed studies.

II. ANALYTICAL DIFFRACTION MODEL

A. Background to scattering problems

The scattering of sound by an object in a uniform and nonviscous medium is characterized by the corresponding pressure distribution, particularly in the region of the scatterer. This can be decomposed into an incident and a scattered field, both of which are governed by the scalar wave equation. In the case of a locally reactive sphere in an infinite medium, for a given incident wave the scattered field is entirely determined by the boundary condition imposed on the surface of the scatterer. This surface boundary condition can be examined using the notion of acoustic impedance (the ratio of surface pressure to radial velocity). The term is dependent on the acoustic properties of the boundary and surrounding fluid, and by definition is time invariant. Of particular interest is whether a material can be considered to be locally reactive. This requires that there is no significant wave motion in the direction tangent to the surface. The motion of the surface at any point can then be considered dependent only on the incident acoustic pressure at that location. While the angle of refraction within the material is dependent on the specific macroscopic material properties, it follows that if the surface material is reasonably dense (greater than $\sim$150 kg/m^3) then over the frequency range of interest a locally reactive boundary condition is a reasonable assumption (Ingard, 1981).

The boundary condition for a sphere of radius a with a locally reacting and uniformly distributed normal acoustic impedance $\mathrm{Z}(\omega)$ is given by

$$0 = \left[\frac{\partial p}{\partial r} + \left(i\rho_0 \omega \frac{1}{\mathrm{Z}(\omega)} \right) p \right]_{r=a}. \tag{1}$$

Here p is the sound pressure, ρ_0 is the mean medium density, ω is the angular frequency, and harmonic time dependence of the form $e^{-i\omega t}$ has been assumed. Impedance values are commonly discussed in their normalized form:

$$\zeta = \frac{Z}{\rho_0 c_0} = \theta + i\chi, \tag{2}$$

where ζ represents the specific acoustic impedance with resistive and reactive components θ and χ, c_0 the wave speed, and $\rho_0 c_0$ the characteristic impedance of the medium. Care must be taken when investigating impedance to ensure that consistent use of the harmonic time component is maintained between impedance measurements and analytical solutions. Using $e^{-i\omega t}$, most common acoustic materials will have a positive impedance phase angle over the frequency range of interest as the stiffness of the material dominates the response.

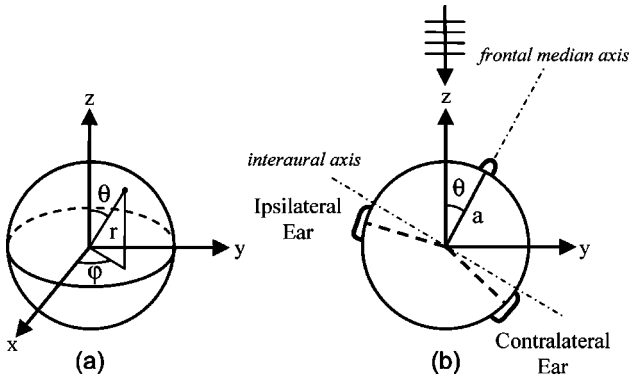

FIG. 1. (a) General spherical coordinate system. (b) Symmetrical coordinate system with incident wave in the negative z direction. The pinnae are offset from the frontal median axis by 100°.

B. Derivation of pressure equation

A general solution for the scalar wave equation (assuming a harmonic time dependence) in spherical coordinates as shown in Fig. 1(a) can be expressed as

$$p = p_0 e^{-i\omega t} \sum_{n=0}^{\infty} \sum_{m=-n}^{n} G_n(r) Y_n^m(\theta, \varphi). \tag{3}$$

Here $G_n(r)$ represents a solution to the spherical Bessel differential equation (which constitutes a linear combination of spherical Bessel, spherical Neumann, or spherical Hankel functions), and $Y_n^m(\theta, \varphi)$ represents the spherical harmonic function. When considering scattering around a single sphere with a uniformly distributed boundary condition, the solution is axially symmetric. As a result the spherical harmonic component of the solution reduces to a Legendre polynomial that depends only on the cosine of the angle between the source and the evaluation position. The corresponding expression for a planar incident wave traveling in the negative z direction is

$$p_i = p_0 e^{-i\omega t} \sum_{n=0}^{\infty} (-i)^n (2n+1) j_n(kr) P_n(\cos\theta), \tag{4}$$

where θ and r define the evaluation position relative to the incident wave using the spherical coordinate system shown in Fig. 1(b), k is the wave number, P_n the Legendre polynomial, and j_n the spherical Bessel function of the first kind which is a solution to the Bessel equation that is finite at the origin. Similarly the expression for the scattered wave is

$$p_s = e^{-i\omega t} \sum_{n=0}^{\infty} A_n h_n^{(1)}(kr) P_n(\cos\theta), \tag{5}$$

where $h_n^{(1)}$ is the spherical Hankel function of the first kind. This represents a solution to the Bessel equation that satisfies the Sommerfeld radiation condition. The singularity of the spherical Hankel function at the origin implies that the sphere must have a finite size.

The constant A_n in Eq. (5) is solved using the boundary condition imposed on the surface of the sphere. Using the locally reactive and uniformly distributed boundary condition described in Eq. (1) yields the complete expression for the sound pressure due to the existence of the sphere in the propagation medium:

$$(p_i + p_s) = p_0 e^{-i\omega t} \sum_{n=0}^{\infty} (-i)^n (2n+1) P_n(\cos\theta) B_n, \tag{6}$$

where

$$B_n = j_n(kr) - \frac{h_n^{(1)}(kr)\left(j_n'(ka) + i\rho_0 c \frac{1}{Z(\omega)} j_n(ka)\right)}{h_n'^{(1)}(ka) + i\rho_0 c \frac{1}{Z(\omega)} h_n^{(1)}(ka)}, \tag{7}$$

and the $(\prime)$ operator denotes the radial derivative.

The interaural azimuth cues are derived from pressure values on the surface of the sphere and Eq. (7) simplifies significantly for $r=a$ using the recursion and cross product relationships for spherical Bessel functions. This yields the surface pressure function:

$$(p_i + p_s)_{r=a} = p_0 e^{-i\omega t} \frac{1}{(ka)^2} \sum_{n=0}^{\infty} \frac{(-i)^{n-1}(2n+1) P_n(\cos\theta)}{h_n'^{(1)}(ka) + i\rho_0 c \frac{1}{Z(\omega)} h_n^{(1)}(ka)}. \tag{8}$$

For a rigid sphere the impedance value becomes infinite and Eq. (8) reduces to yield the solution for the rigid boundary condition as presented and discussed by many previous authors (e.g., Blauert, 1997).

C. Extraction of azimuth cues

The two primary auditory cues for discerning sound source direction in the azimuth plane are the ILD and the ITD. These cues can be analytically derived from Eq. (8) using the known locations of the pinnae which are offset from the frontal median axis by 100° as shown in Fig 1(b). The ILD is obtained by examining the difference in sound pressure level between the two pinna locations:

$$\mathrm{ILD} = 20 \log_{10}\left(\left| \frac{(p_i + p_s)_{\text{ipsilateral ear}}}{(p_i + p_s)_{\text{contralateral ear}}} \right| \right). \tag{9}$$

Similarly the ITD for each angle of incidence is calculated from the interaural difference in arrival time. The actual analytical value of ITD differs slightly depending on the method used to derive this time delay. Interaural phase delay and group delay are frequently used and exhibit similar characteristics but both are frequency dependent and display an increase in ITD at low frequencies (Kuhn, 1977). Ray tracing algorithms (Woodworth and Schlosberg, 1954), amplitude threshold based time constants (Duda and Martens, 1998), or comparisons to minimum phase reconstructions (Kulkarni *et al.*, 1995) can alternatively be used to derive a single value for interaural time difference for each source angle. The ITD is calculated here using a frequency averaged interaural

phase delay. For a particular location on the sphere this phase delay is computed using the negative of the phase response $\Theta(\omega)$ divided by the angular frequency:

$$D(\omega) \triangleq -\frac{\Theta(\omega)}{\omega}. \tag{10}$$

The ITD is then computed from the difference in this delay (averaged across the frequency range of interest) between the two pinna locations. Since the monaural resonant effects of the pinna cavity begin to appear in an experimental HRTF above 3000 Hz, implementations of composite HRTFs generally utilize the analytical model only for frequencies up to this point. The phase delay average is hence calculated over a frequency range from 100 to 3000 Hz. This has the effect of proportionally increasing the ITD values when compared to those obtained from averages over a larger frequency range, or those found using some of the alternative measures mentioned previously. This increase is due to the augmented effect of the larger phase delay below 1000 Hz; however the observed trends due to the impedance inclusion are considered consistent regardless of this selection.

III. EXPERIMENTAL COMPARISON

A. Equipment and setup

The surface pressure function Eq. (8) was validated through a series of interaural measurements completed in an anechoic chamber. A rotating wooden sphere of radius 0.124 m (supported by a thin steel rod) was used which contained two internal microphone cavities (without pinnae), each offset from the frontal median axis by 100°. The angle of the frontal median sphere axis relative to the sound source was aligned using a laser level positioned at the base of the sound source (located approximately 3 m from the sphere) in conjunction with degree markings on the rotating sphere stand. The 0° marking was initially aligned such that an ITD of approximately 0 was obtained. Exposed areas of the stand were covered with a thick layer of highly absorbent material to minimize additional reflections.

A felt covering (190 kg/m^3, 10.3 mm thick) was used to investigate the changes in interaural cues derived from a sphere with a nonrigid boundary condition. This material was selected based on its varying acoustic characteristics throughout the frequency range of interest, its conformity to the locally reactive surface assumption, availability, and its ability to be crafted into a suitable form to use as a covering for the wooden test sphere. The covering was constructed such that the material fitted tightly but was not deformed to any significant degree. Small circular holes were cut in the material coincident with the microphone locations to enable microphone placement flush with the outer material surface (although repeat experiments showed that this placement was not critical). Comparison impedance measurements of both the wood and felt materials were conducted using the two microphone impedance tube method according to the ISO 10534-2 standard (ISO 10534-2, 1998). Figure 2(a) shows the absorption characteristics of the materials (including the rigid steel backing plate of the impedance tube), and Fig. 2(b) shows the resistive and reactive components of the specific impedance of the felt test material.

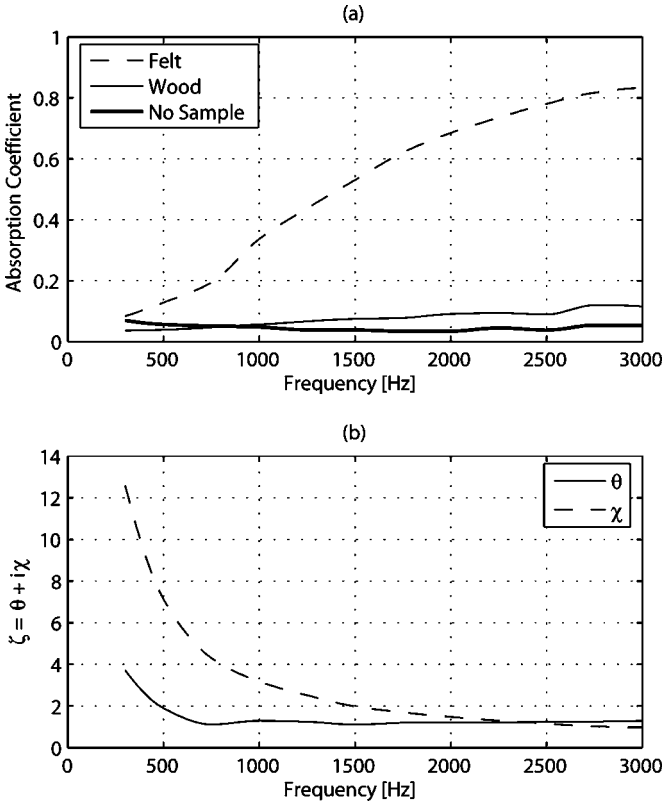

FIG. 2. Measured acoustical properties of the 190 kg/m^3 felt test material. (a) Absorption coefficient with reference to the properties of the wooden test material and steel impedance tube termination. (b) Resistive (θ) and reactive (χ) components of the specific acoustic impedance ζ as defined in Eq. (2).

For each test the microphones (BSWA Tech - MP205 tip, MA211 inline preamplifier) were positioned flush with the exterior of the outer sphere surface. Impulse response measurements were obtained at 5° increments of sphere rotation angle using maximum length sequences produced by the Brüel & Kjær DIRAC software and a Brüel & Kjær HP1001 unidirectional sound source. A sequence length of $2^{14}-1$ (the shortest available sequence length) with 10 averages and a sampling frequency of 48000 Hz was used. To remove the effects of the acoustic measurement environment the impulse response peak onsets were located and the tails truncated to 64 samples. The complete impulse responses were then shortened to 128 samples (with the timing information preserved) and converted to the frequency domain using a 256 point FFT.

B. Interaural comparisons

A comparison between ITD values derived analytically using the measured impedance values and those obtained experimentally is shown in Fig. 3. These results show a strong agreement for both the wooden and felt surfaces. The addition of the felt test surface to the wooden sphere causes an increased sphere radius, and approximately 55% of the difference in ITD between the wooden and felt surfaces is due to this change. The remainder is due to the impedance

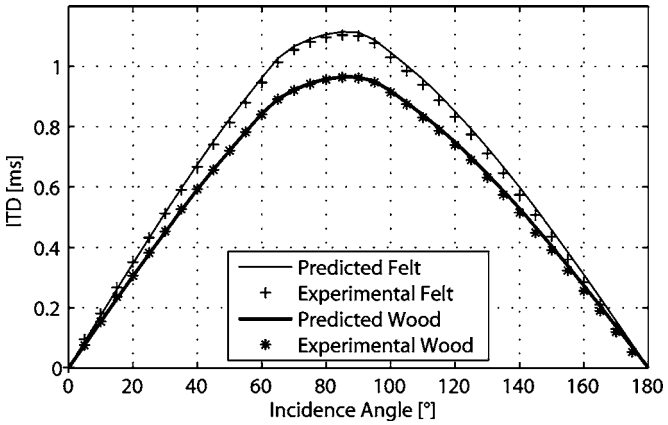

FIG. 3. Comparison between experimental and predicted values of interaural time difference (ITD) for the wood and felt sphere surfaces.

characteristics of the felt. Analytical comparisons for the felt test surface were made using this increased radius (0.135 m).

The experimentally measured change in ILD due to the addition of the felt covering is shown in Fig. 4(a). Again this result matches the predicted changes shown in Fig. 4(b) extremely well. The match between experimental and theoretical results suggests that Eq. (8) provides a strong analytical basis for the derivation of the azimuthal cues experienced by a single sphere with a uniformly distributed surface impedance.

IV. GENERAL TRENDS

A. Effect of impedance on the sphere surface pressure

Experimental comparisons shown and discussed in Sec. III validate the use of the analytical treatment presented in Sec. II for investigating the general effect of impedance on the interaural cues derived from a single sphere. The effects of varying two fundamental aspects of acoustic impedance (magnitude and phase) are investigated here independently. For convenience the general trends in derived interaural differences are examined using frequency independent values of impedance. Results and discussion relating to changes in azimuth cues due to the impedance of human hair (frequency dependent impedance) are given in Sec. V. A sphere radius of 0.0875 m is assumed throughout the remainder of the paper.

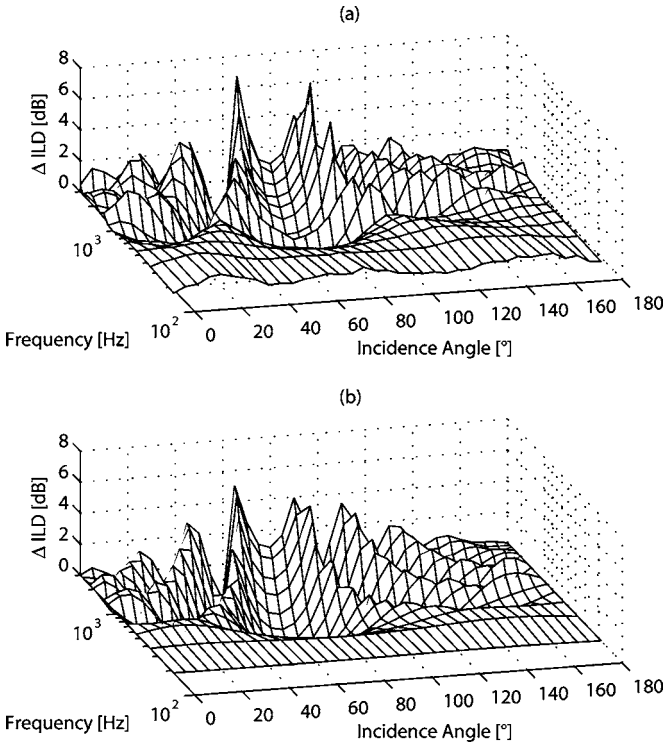

FIG. 4. Comparison between (a) experimental and (b) predicted values of the change in interaural level difference (ΔILD) due to the felt surface.

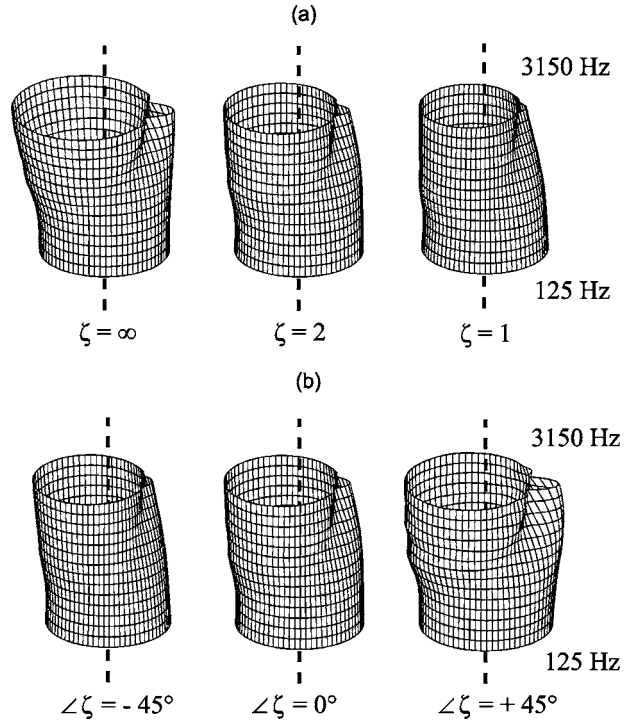

FIG. 5. Sphere surface pressure with changes in (a) resistive specific impedance ζ, and (b) complex specific impedance phase angle $\angle\zeta$ for a constant magnitude of $|\zeta|=2$. The incident wave approaches from the left and each horizontal layer represents the surface pressure at a particular frequency from 125 to 3150 Hz in 1/3 octave band increments. The dashed line indicates the polar origin and the bottom layer (125 Hz) is approximately the unit circle.

Figure 5(a) illustrates the effect of decreasing the magnitude of a purely resistive impedance from an infinite value ($\zeta=\infty$), to the characteristic impedance of air ($\zeta=1$), on the magnitude of the sphere surface pressure. The cylindrical shapes represent stacked polar plots, with each horizontal slice corresponding to the pressure distribution around the sphere circumference at a particular frequency. The frequency spacing corresponds to one-third-octave bands in the range from 125 to 3150 Hz, and the angular spacing is 5°. The incident wave approaches from the left, and the dashed line indicates the polar origin. Consistent with previous investigations of sphere scattering, the response at low frequencies is approximately unity (Morse and Ingard, 1968). This provides a convenient reference for examining the trends at higher frequencies. When the sphere is rigid ($\zeta=\infty$) as the frequency increases the surface pressure in the anterior region begins to approach double the free-field response. This is consistent with expectations of reflection from a rigid plane. In compliance, the response in the poste-

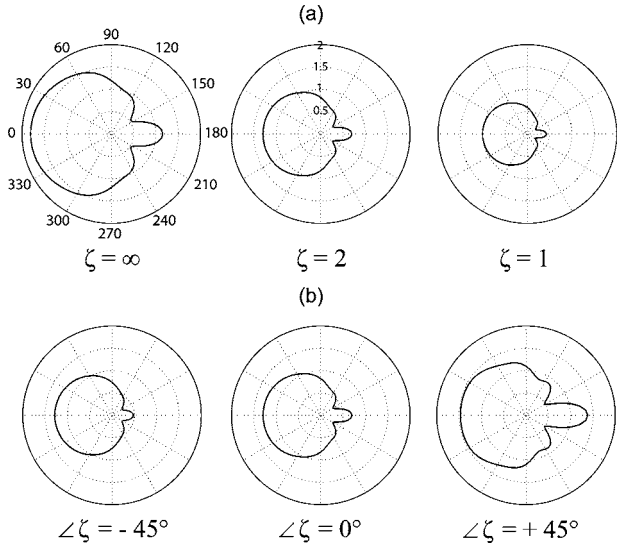

FIG. 6. Sphere surface pressure at $f=2000$ Hz with changes in (a) resistive specific impedance ζ, and (b) complex specific impedance phase angle $\angle\zeta$ for a constant magnitude of $|\zeta|=2$. These polar plots correspond to the third uppermost horizontal slice of the stacked polar plots shown in Fig. 5.

rior region reduces. The lobe of increased pressure at the rear of the sphere is a result of symmetrically diffracted waves arriving in phase creating a "bright spot" (Duda and Martens, 1998). At higher frequencies other small lobes of increased pressure can be seen on either side of the most prominent bright spot resulting from the same phenomena. The angular location of these ancillary lobes is dependent on frequency. Quantitative comparison of the changes in surface pressure for $f=2000$ Hz is possible using Fig. 6(a). These polar plots correspond to the third uppermost horizontal slice of the stacked polar plots shown in Fig. 5(a).

As the magnitude of the resistive surface impedance is decreased, there is an overall decrease in the sphere surface pressure level. There is a particularly significant reduction in the region of the bright spot, proportionally more so than for frontal regions. This is a result of the increased absorption of the sphere surface reducing the intensity of the reflected sound which has a compounding effect on the level of sound that is diffracted to the rear of the sphere. This trend is consistent with previous empirical observations regarding head scattering and impedance, particularly in relation to hair (Katz, 2001; Riederer, 2005).

When the surface impedance also contains a reactive component, the interaction of the incident wave with the sphere boundary causes a phase difference in the reflected wave. This change consequently alters both the resultant sound pressure on and around the sphere, and the corresponding interaural cues. Figure 5(b) illustrates the change in sphere surface pressure with impedance phase angle $\angle\zeta$ while keeping the overall impedance magnitude constant at a value of $|\zeta|=2$. The corresponding polar plots for $f=2000$ Hz are shown in Fig. 6(b). Again the most significant changes are in the posterior region of the sphere. For a negative impedance phase angle (positive resistive component, negative reactive component) the out-of-phase reflected waves produce a further reduction in the sound diffracted to the rear sphere surface. Conversely a positive impedance

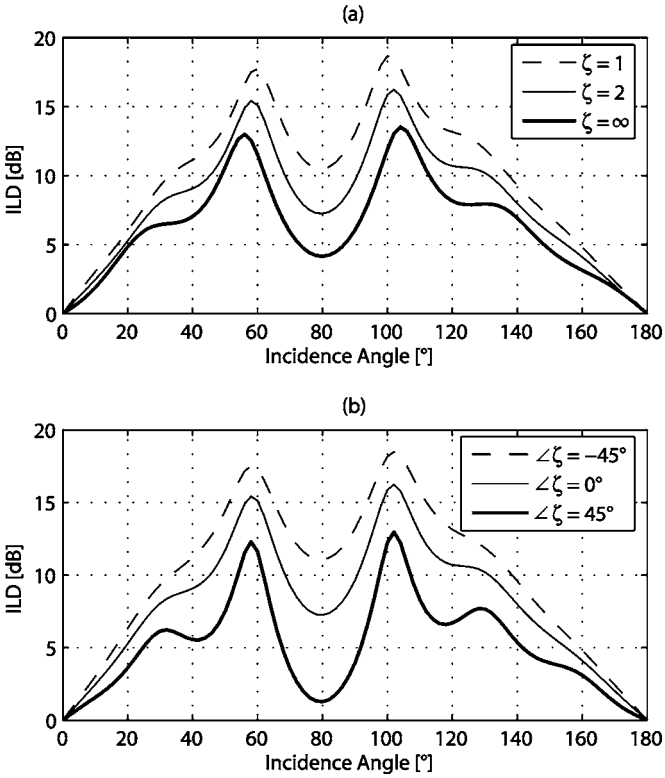

FIG. 7. ILD changes at 3000 Hz with (a) changes in resistive specific impedance and (b) changes in impedance phase angle for constant magnitude of $|\zeta|=2$.

phase angle increases the magnitude of the bright spot lobes in a particularly significant manner. For both cases the effect is less pronounced at lower frequencies.

B. Effect of impedance on the interaural level difference

Figure 7(a) illustrates the resulting changes in ILD at 3000 Hz with a reduction of resistive impedance magnitude. The general decrease in level difference at 80° for all curves is a result of the contralateral ear (offset from the frontal median axis by 100°) being coincident with the principal bright spot. As the impedance magnitude is decreased, the surface pressure reduction in the posterior region of the sphere results in a more pronounced level difference between opposing pinnae, particularly for source directions near the interaural axis. The same trend is exhibited at other frequencies; however below 500 Hz the effect is less significant because the augmented diffraction begins to reduce the ILD to a negligible amount. Figure 7(b) illustrates the resulting effect of the impedance phase angle for a constant magnitude $|\zeta|=2$ on the ILD. A negative phase angle produces an increased ILD in a similar manner to that shown in Fig. 7(a). A positive phase angle produces a decrease, however of particular interest is the amplified decrease for source angles where the contralateral ear coincides with a bright spot of increased magnitude.

Over the frequency range of interest the acoustic properties of most common materials will be governed by their stiffness, and as a result impedance values will have a positive phase angle. The overall decrease in the posterior sur-

face pressure due to the absorption characteristics of the material will be counteracted by the increase in the bright spot lobes due to the positive impedance phase angle. This effect can be seen in Fig. 4 where the change in ILD is positive for source angles where the contralateral ear coincides with a reduction in surface pressure (due to the decreased impedance magnitude), and negative for source angles where it coincides with a bright spot lobe of increased magnitude (due to the positive impedance phase angle). At higher frequencies (in particular those beyond the investigated frequency range) the reduction in posterior surface pressure due to the material absorption becomes dominant. Additionally at these frequencies many materials become governed by their mass properties (and hence the impedance will have a negative phase angle) which further consolidates this effect.

Previous studies into sound localization have shown that when ITD and ILD cues conflict, the ITD cue takes precedence on listeners' judgment of sound direction (Wightman and Kistler, 1992; Macpherson and Middlebrooks, 2002). This is particularly true for low frequencies where there is a limited ILD. It is generally believed that for wideband or low-pass stimuli, the ITD is used to establish the general azimuthal direction, and ILD and monaural spectral cues used to resolve any ambiguities (Shinn-Cunningham *et al.*, 2000). Under these conditions even when the ILD is biased by more than 10 dB, there is little effect on the overall perceived sound direction, although the number of front-back confusions substantially increases for very large ILD biases (Wightman and Kistler, 1997; Macpherson and Middlebrooks, 2002). The change in ILD due to the surface impedance is thus not considered significant in regards to a concrete change in apparent stimulus direction; however an ILD well matched to a modified ITD cue will increase the fidelity of any subsequent virtual 3D projection.

C. Effect of impedance on the interaural time difference

The interaural time difference cue is generally more impervious to system changes than the level difference [for example, for near-field sources (Duda and Martens, 1998)] and this trend continues here and is consistent with the primacy of the ITD as an azimuthal auditory cue when conflicts occur. Figure 8 illustrates the change in ITD with the magnitude of a purely resistive impedance (calculated from the frequency averaged time delay). A general increase in ITD is seen with a decrease in the impedance magnitude, particularly for source angles near the interaural axis. Here the difference in ITD between a completely rigid and highly absorptive sphere is around 100 μs. This difference is enough to shift the perceived source direction by as much as 20°, a value which is significantly more than previously published values for spatial resolution around the interaural axis (Blauert, 1997; Grantham *et al.*, 2003). For source directions closer to the median axis the change in ITD is reduced, however the minimum audible angle threshold in this region is also reduced. Altering the phase angle of the sphere impedance in either direction produces a reduction in ITD. This reduction is a maximum for impedance phase angles of ±90°, and for source angles near the interaural axis (40 μs

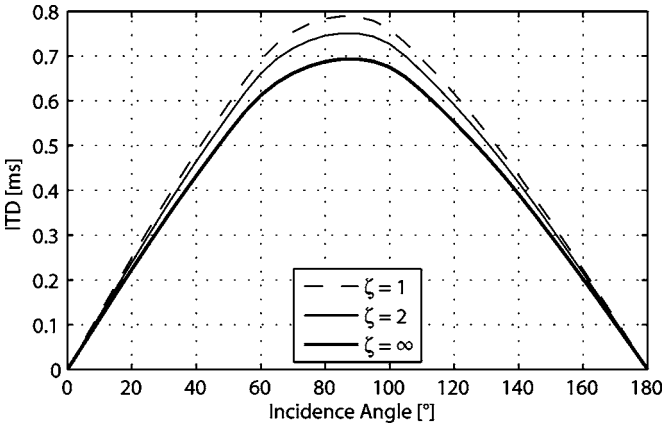

FIG. 8. Interaural time difference (ITD) changes with changes resistive specific impedance value.

for an impedance magnitude of $|\zeta| = 2$).

V. THE EFFECT OF HUMAN HAIR

A. Impedance characteristics of hair

Under natural conditions, human hair is generally of low density and is reasonably porous in composition. Using an impedance tube to measure normal impedance values at an approximated frontal hair surface results in calculated characteristics close to that of air (especially for sparsely populated samples). If the material has a particularly low bulk modulus, the speed of sound propagation through it can become less than c_0 and values of impedance $\xi < 1$ can occur. Using the acoustic properties of hair measured under these conditions with Eq. (8) will not give an accurate description of the surface boundary condition as the sphere (head) is not entirely constituted of the hair material (and if it were flow within the material could not be ignored). The impedance value used must account for the relatively thin layer of the hair material on an approximately rigid backing. To satisfy this requirement, measured values of hair impedance were assumed to be equal to the impedance at the rigid tube termination with the hair sample placed in front. A comparison between locally and nonlocally reacting limp porous layers on a rigid backing is given by Ingard (1981). This study suggests that over the frequency range investigated in the current work, locally and nonlocally reacting layers exhibit similar properties (with slightly improved absorption characteristics evident for the nonlocally reacting layer). Considering the relatively small thickness of the hair layer a locally reactive boundary condition is believed to be a valid assumption.

The properties of three separate hair samples of varying length (15–40 mm) and hair type [medium thickness circular cross section, fine thickness circular cross section, and medium thickness oval cross section (curly)] were measured using the two microphone methodology under the surface assumption described earlier. Samples were aligned arbitrarily in a sample holder (20 mm deep, 60 mm in diameter with a fine mesh front) at three different densities. Figure 9(a) shows the averaged results of absorption coefficient for each density. These match well with previously published

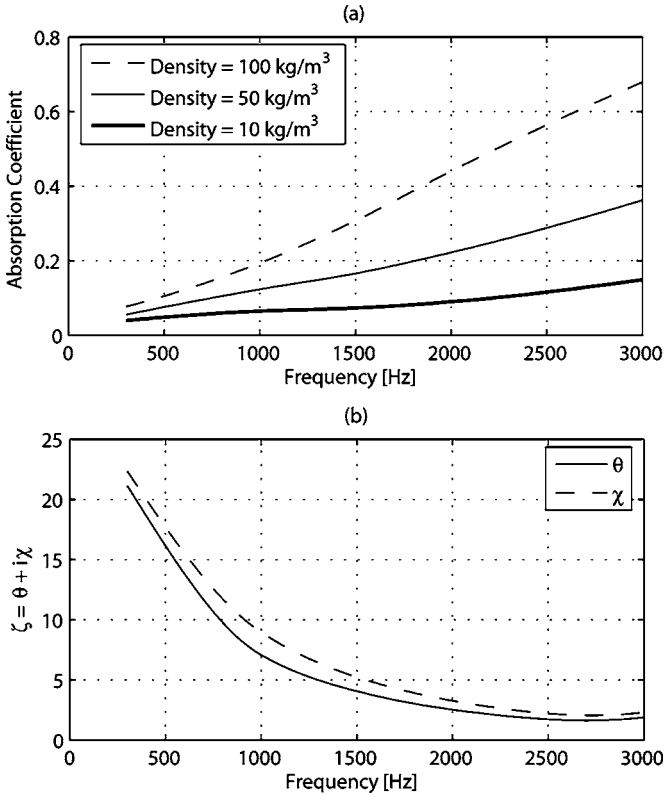

FIG. 9. Measured acoustical properties of human hair in a 20-mm-deep sample holder. (a) Absorption coefficient with varying density. (b) Resistive (θ) and reactive (χ) components of the specific acoustic impedance (ζ) of hair at 100 kg/m^3.

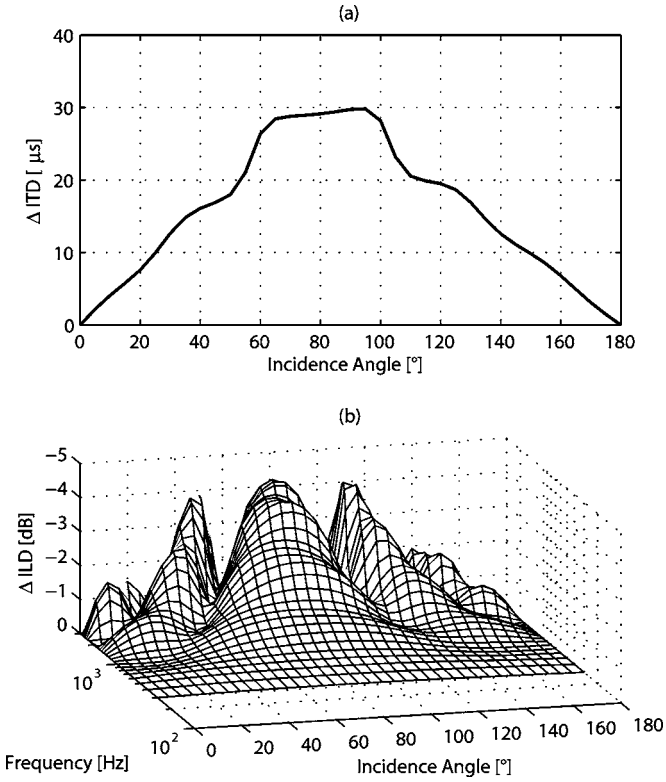

FIG. 10. Predicted changes in (a) ITD and (b) ILD due to the impedance of hair with 100 kg/m^3 density.

hair absorption coefficient data for sample densities of 86–255 kg/m^3 and a sample depth of 15 mm (Katz, 2000). Between sample comparisons provided remarkably consistent results suggesting that the length and type of hair have little effect on the acoustical properties. This is consistent with observations by Riederer (2005).

Figure 9(b) illustrates the resistive and reactive components of the specific impedance for a density of 100 kg/m^3 (again averaged across the three hair samples). The decrease in both the resistive and reactive components with frequency illustrates the increasing absorption. The similarity between the resistive and reactive components results in a relatively consistent positive impedance phase angle of approximately 50°.

B. Changes to interaural cues

Figure 10 illustrates the change in ITD and ILD due to the impedance characteristics of hair. The prediction is made under a locally reactive and uniformly distributed boundary condition assumption using the impedance of hair at a density of 100 kg/m^3 as shown in Fig. 9(b). For source directions near the interaural axis there is an increase in ITD of around 30 μs. Due to the frequency dependent nature of the impedance characteristics, little change is seen in the low-frequency component of the phase delay. This reduces the impact of the impedance on the ITD, which is calculated from the frequency averaged interaural phase delay. For sources lacking in low-frequency information (below 1000 Hz), the change in ITD is more prominent, although at higher frequencies the contribution of the ILD is also more significant.

Published values for just-noticeable-difference changes in the ITD vary depending on the frequency content of the source, and the reference ITD. These range from 10 to 100 μs, with the smaller values generally corresponding to reference ITDs closer to 0, or experiments using pure tones, particularly those at lower frequencies (Mossop and Culling, 1998). Depending on the nature of the hair surface and the listening experiment, including the effects of hair impedance may thus produce a small but noticeable shift in the perceived source direction. The change in ILD due to the inclusion of hair characteristics is shown in Fig. 10(b). Again this change is most significant for source directions close to the interaural axis, with differences on the order of 4 dB. While the magnitude of the changes in ITD and ILD exhibited due to the effect of hair are seemingly small, they are of similar order to changes reported from previous empirical studies into the effect of impedance (Kuhn, 1977; Katz, 2001; Riederer, 2005).

VI. CONCLUSION

The results of experimental validation show that a sphere diffraction model based on a locally reactive and uniformly distributed boundary condition provides a proficient foundation for predicting the changes to the surface pressure and interaural cues in the azimuth plane when the surface is not rigid. Using this model with varying surface impedance gives insight into the behavior of the surface pressure from

which the interaural cues are derived. Decreasing the magnitude of a purely resistive surface impedance results in an overall decrease in the sphere surface pressure level, particularly in the posterior region. This results in nontrivial increases in both the ITD and ILD, especially for sound source directions near the interaural axis. When the surface impedance is complex, the impedance phase angle dictates further changes to the surface pressure and interaural cues. For a negative impedance phase angle the surface pressure exhibits a further decrease. For a positive impedance phase angle the posterior surface pressure exhibits an increase in the magnitude of bright spot lobes (which result from symmetrically diffracted waves arriving in phase). This results in a decrease in the ILD, particularly when the contralateral ear coincides with the location of a bright spot lobe. The ITD is slightly decreased with modification of the impedance phase angle in either direction, with the maximum reduction occurring for a purely reactive surface impedance and source directions near the interaural axis.

Over the frequency range investigated in this study the impedance properties of most acoustic materials will be dictated by their stiffness. This results in a positive impedance phase angle and the decrease in surface pressure in the posterior region of the sphere due to the material absorption will be offset by the increase in the bright spot lobes. Both positive and negative shifts in ILD are therefore possible depending on the exact properties of the scattering surface. At higher frequencies (particularly beyond the range formally investigated in this study) the reduction in surface pressure due to absorption dominates. Additionally at these frequencies many materials are also commonly mass controlled and the decrease in the posterior surface pressure is consolidated by the negative impedance phase angle. This result may be significant for any modeling which utilizes the sphere diffraction solution at higher frequencies (for example, structural models which separately account for head, torso, and pinnae effects). Under the locally reactive and uniformly distributed boundary assumption the impedance characteristics of human hair of density 100 kg/m^3 produce changes in ILD and ITD on the order of 4 dB and 30 μs which are comparable with just-noticeable-difference thresholds.

While the analytical diffraction model presented in this paper is not adequately equipped to directly deal with surfaces of multifaceted impedances, the impetus and significance of the investigation was to examine whether modifying the surface boundary condition would modify the interaural cues to an extent that would warrant further investigation. As hair only covers the upper and rear portion of head surface, it is predicted that the actual changes due to the impedance characteristics of hair would be proportionally less. The presented model thus cannot necessarily provide an accurate direct replacement for the sphere diffraction models that are currently used to compute interaural parameters. A useful annexure and interesting physical study would be to solve the wave equation based on a sphere with position dependent impedance (as is possible for finite and boundary element computational models). This would provide a more accurate account of the effect of the surface impedance characteristics on the low-frequency interaural cues, and insight into the physical mechanisms of scattering around a human head with hair.

ACKNOWLEDGMENTS

B.E.T. would like to acknowledge the support of the Robert and Maude Gledden, and F S Shaw Memorial Postgraduate Scholarships. The insightful questions and comments by the anonymous reviewers and the associate editor were also appreciated.

Algazi, V. R., Avendano, C., and Duda, R. O. (**2001**). "Estimation of a spherical-head model from anthropometry," J. Audio Eng. Soc. **49**, 472–479.

Algazi, V. R., Duda, R. O., Duraiswami, R., Gumerov, N. A., and Tang, Z. (**2002a**). "Approximating the head-related transfer function using simple geometric models of the head and torso," J. Acoust. Soc. Am. **112**, 2053–2064.

Algazi, V. R., Duda, R. O., and Thompson, D. M. (**2002b**). "The use of head-and-torso models for improved spatial sound synthesis," *Proceedings of the 113th AES Convention*, Audio Engineering Society, Los Angeles, CA, preprint 5712.

Blauert, J. (**1997**). *Spatial Hearing: The Psychophysics of Human Sound Localization* (MIT, Cambridge, MA).

Bronkhorst, A. W. (**1995**). "Localization of real and virtual sources," J. Acoust. Soc. Am. **98**, 2542–2553.

Brown, C. P., and Duda, R. O. (**1998**). "A structural model for binaural sound synthesis," IEEE Trans. Speech Audio Process. **6**, 476–488.

Duda, R. O., and Martens, W. L. (**1998**). "Range dependence of the response of a spherical head model," J. Acoust. Soc. Am. **104**, 3048–3058.

Grantham, D. W., Hornsby, B. W. Y., and Erpenbeck, E. A. (**2003**). "Auditory spatial resolution in horizontal, vertical, and diagonal planes," J. Acoust. Soc. Am. **114**, 1009–1022.

Gumerov, N. A., and Duraiswami, R. (**2002**). "Computation of scattering from *N* spheres using multipole reexpansion," J. Acoust. Soc. Am. **112**, 2688–2701.

Ingard, K. U. (**1981**). "Locally and nonlocally reacting flexible porous layers; A comparison of acoustical properties," J. Eng. Ind. **103**, 302–313.

ISO 10534-2 (**1998**). Determination of Sound Absorption Coefficient and Impedance in Impedance Tube. 2. Transfer-Function Method (ISO).

Katz, B. F. G. (**2000**). "Acoustic absorption measurement of human hair and skin within the audible frequency range," J. Acoust. Soc. Am. **108**, 2238–2242.

Katz, B. F. G. (**2001**). "Boundary element method calculation of individual head-related transfer function. II. Impedance effects and comparison to real measurements," J. Acoust. Soc. Am. **110**, 2449–2455.

Kear, G. (**1959**). "The Scattering of Waves by a Large Sphere for Impedance Boundary Conditions," Ann. Phys. (N.Y.) **6**, 102–113.

Kuhn, G. F. (**1977**). "Model for the interaural time differences in the azimuthal plane," J. Acoust. Soc. Am. **62**, 157–167.

Kulkarni, A., Isabelle, S. K., and Colburn, H. S. (**1995**). "On the minimum-phase approximation of head-related transfer functions," *IEEE ASSP Workshop on Applications of Signal Processing to Audio and Acoustics, 1995*, (IEEE, New Paltz, New York), pp. 84–87.

Lax, M., and Feshbach, H. (**1948**). "Absorption and scattering for impedance boundary conditions on spheres and circular cylinders," J. Acoust. Soc. Am. **20**, 108–124.

Macpherson, E. A., and Middlebrooks, J. C. (**2002**). "Listener weighting of cues for lateral angle: The duplex theory of sound localization revisited," J. Acoust. Soc. Am. **111**, 2219–2236.

Middlebrooks, J. C. (**1999**). "Virtual localization improved by scaling nonindividualised external ear transfer functions in frequency," J. Acoust. Soc. Am. **106**, 1493–1510.

Middlebrooks, J. C., Macpherson, E. A., and Onsan, Z. A. (**2000**). "Psychophysical customization of directional transfer functions for virtual sound localization," J. Acoust. Soc. Am. **108**, 3088–3091.

Morse, P. M., and Ingard, K. U. (**1968**). *Theoretical Acoustics* (McGraw-Hill, New York).

Mossop, J. E., and Culling, J. F. (**1998**). "Lateralization of large interaural delays," J. Acoust. Soc. Am. **104**, 1574–1579.

Riederer, K. A. J. (**2005**). "HRTF analysis: Objective and subjective evalu-

ation of measured head-related transfer functions," Helsinki University of Technology, Helsinki.
Shinn-Cunningham, B. G., Santarelli, S., and Kopco, N. (**2000**). "Tori of confusion: Binaural localization cues for sources within reach of a listener," J. Acoust. Soc. Am. **107**, 1627–1636.
Wenzel, E. M., Arruda, M., Kistler, D. J., and Wightman, F. L. (**1993**). "Localization using nonindividualized head-related transfer functions," J. Acoust. Soc. Am. **94**, 111–123.
Wightman, F. L., and Kistler, D. J. (**1992**). "The dominant role of low-frequency interaural time differences in sound localization," J. Acoust. Soc. Am. **91**, 1648–1661.
Wightman, F. L., and Kistler, D. J. (**1997**). "Monaural sound localization revisited," J. Acoust. Soc. Am. **101**, 1050–1063.
Woodworth, R. S., and Schlosberg, H. (**1954**). *Experimental Psychology* (Holt, New York).
Zotkin, D. N., Hwang, J., Duraiswami, R., and Davis, L. S. (**2003**). "HRTF personalization using anthropometric measurements," *IEEE Workshop on Applications of Signal Processing to Audio and Acoustics, 2003* (IEEE, New Paltz, NY), pp. 157–160.